www.adeepakpublishing.com

Clements, E. et al. (2019): JoSS, Vol. 8, No. 1, pp. 815–836
(Peer-reviewed article available at www.jossonline.com)

www. JoSSonline.com

Lasercom Uncertainty Modeling and Optimization Simulation (LUMOS): A Statistical Approach to Risk-Tolerant Systems Engineering for Small Satellites

Emily Clements, Jeffrey Mendenhall, and David Caplan

MIT Lincoln Laboratory
Lexington, MA US

Kerri Cahoy

Massachusetts Institute of Technology
Cambridge, MA US

Abstract

In contrast to large-budget space missions, risk-tolerant platforms such as nanosatellites may be better positioned to exchange moderate performance uncertainty for reduced cost and improved manufacturability. New uncertainty-based systems engineering approaches such as multidisciplinary optimization require the use of integrated performance models with input distributions, which do not yet exist for complex systems, such as laser communications (lasercom) payloads. This paper presents our development of a statistical, risk-tolerant systems engineering approach and apply it to nanosatellite-based design and architecture problems to investigate whether adding a statistical element to systems engineering enables improvements in performance, manufacturability, and cost. The scope of this work is restricted to a subset of nanosatellite-based lasercom systems, which are particularly useful given current momentum to field Earth-observing nanosatellite constellations and increasing challenges for data retrieval. We built uncertainty-based lasercom performance models for a low Earth orbiting (LEO) system being developed at MIT called the Nanosatellite Optical Downlink Experiment (NODE) as a reference architecture. Compared with more traditional, deterministic systems engineering, we find that our new Lasercom Uncertainty Modeling and Optimization Simulation (LUMOS) approach yields significant benefits, including a lasercom downlink design with a 59% reduction in ground station diameter and a 46% reduction in space terminal power for equivalent probabilities of a LEO-ground system delivering 500 Gb/day. While this study focuses on a nanosatellite lasercom application, the process for characterizing the input distributions and modeling performance is generalizable to other lasercom systems or space systems.

1. Introduction

Nanosatellite[1] systems engineering can benefit from using an uncertainty-based design methodology, which has been shown to improve decision-making for complex systems (De Neufville et al., 2004). Systems engineering for nanosatellites can be challenging, because time and resource constraints require design decisions to be made before all risk can be mitigated. While spacecraft programs with larger budgets can

[1] In this paper, the term "nanosatellite" refers to a satellite with a total mass of less than 10 kg (see Buchen, 2014); nanosatellites are usually flown as secondary payloads, although satellite mass categories can vary.

Corresponding Author: Emily Clements – eclements@mit.edu
Publication History: Submitted – 09/18/18; Revision Accepted – 02/27/19; Published – 05/06/19

often design to accommodate worst-case conditions, the on-board size, weight, and power constraints of nanosatellites often do not allow for adding design margin to compensate for uncertainty.

A probabilistic design approach can be particularly useful for complex systems such as laser communications (lasercom) payloads, but implementation is made challenging because modeling or test data are required for every input. Furthermore, input distribution databases are not currently available, making the use of a probabilistic systems engineering approach more time-consuming. Without these databases, the application of a probabilistic approach for these systems has been limited.

We seek to address this gap by adding a statistical component to systems engineering of nanosatellite lasercom systems. We describe the implementation of the new Lasercom Uncertainty Modeling and Optimization Simulation (LUMOS) to support a nanosatellite hyperspectral imaging mission, present architecture-specific input distributions for the link model, and compare the lasercom performance using LUMOS with the expected performance of traditional, deterministic design methodologies (as measured by downlink data volume). The results highlight the potential for achieving better performance using an uncertainty-based approach to risk-tolerant design.

1.1. LUMOS Overview

LUMOS aids decision-making under uncertainty by estimating the probability of achieving specific design goals, rather than estimating lower bounds on system performance (in this case measured by data volume). The LUMOS approach is to develop a database of input distributions for all factors that influence a lasercom link budget, and propagate these uncertainties using Monte Carlo analysis. These Monte Carlo analyses are run for each design vector in a formal design optimization process, and can be used to assess the probability of success and dependence on particular design parameters. Performance metrics are re-framed as probabilistic metrics, e.g., the probability of achieving a desired data volume downlinked per day. The implementation of LUMOS is described in detail in Section 3.

To ensure that LUMOS implementation is relevant and realistic, we apply the model to a reference design called the Nanosatellite Optical Downlink Experiment (NODE), described in detail in Clements et al. (2016). NODE is an ongoing program for demonstrating moderate rate (10–100 Mbps) optical communications downlink from a CubeSat using a 0.2 W, 1550 nm, 1.3 mrad transmitter laser beam. While this work is directly relevant to future generations of NODE, the framework can be updated for other laser communication systems or payloads that are sensitive to similar variations in input conditions.

1.2. Motivation for Modeling Laser Communications

While the probabilistic approach described in this paper could be applied to a variety of nanosatellite design problems (Clements, 2018), this paper focuses on lasercom systems, which are attractive for nanosatellites for several reasons, such as improved power efficiency and spectrum availability, increased capacity, and reduced ground station cost. For long-distance free-space links, lasercom is often more power-efficient than radio frequency (RF) communication, because the shorter optical wavelengths result in a lower beam divergence[2] for a given aperture diameter (see, e.g., Alexander, 1997). Lasercom has also been demonstrated in space on larger spacecraft, such as the Lunar Laser Communication Demonstration (LLCD) (Boroson et al., 2014), Optical Inter-Orbit Communications Engineering Test Satellite (OICETS) (Jono et al., 2006), and the Small Optical TrAnsponder (SOTA) (Takenaka et al., 2016). The Size, Weight, and Power (SWaP) of these missions has exceeded the size of CubeSat communications systems, so miniaturization and/or redesign would be necessary for nanosatellite applications. See Hemmati and Caplan

[2] Beam divergence is proportional to $\frac{\lambda}{D}$, where λ is wavelength and D is the diameter of the transmitter.

(2013) for a list of representative space-based lasercom systems and relevant link parameters.

Several organizations are working on lasercom for nanosatellites. CubeSat demonstration systems include the Optical Communication Sensor Demonstration (OCSD) from the Aerospace Corporation (Rowen et al., 2016; Rowen and Dolphus, 2013),[3] the Nanosatellite Optical Downlink Experiment (NODE) from the Massachusetts Institute of Technology (MIT) (Clements et al., 2016),[4] and the TeraByte InfraRed Downlink (TBIRD) from MIT Lincoln Laboratory (Robinson et al., 2018). Commercial systems are being developed by Sinclair Interplanetary (Sinclair and Riesing, 2017), Fibertek (Mathason et al., 2019), and Gooch & Housego (Crabb et al., 2019). The University of Florida is developing compact modulators (Serra et al., 2015), and the NASA Jet Propulsion Laboratory is developing lasercom for interplanetary missions (Kovalik et al., 2015). DLR is building on recent on-orbit experiments with the OSIRIS instrument on the Flying Laptop small satellite to develop a CubeSat-scale laser communication system (Fuchs et al., 2019). We expect that this list may not be complete, since nanosatellite lasercom is an active area of research and development, and other organizations may have designs in progress.

1.3. Paper Organization

Section 2 of this paper provides background on laser communications and nanosatellite system modeling, and Section 3 describes the implementation of LUMOS for a lasercom design case study. In Section 4, we describe probabilistic modeling results for application examples and how these results may be used in program development. Finally, Section 5 summarizes results and implications, and discusses further relevant applications.

2. State of the Art in Nanosatellite Systems Engineering and Lasercom Modeling

The LUMOS approach builds on integrated modeling and uncertainty management techniques from nanosatellite systems engineering research combined with input characterization from lasercom modeling research.

2.1. Gap in Systems Engineering Methodologies for Balancing Uncertainty with Manufacturability

Systems engineering methodologies for designing under uncertainty have focused on characterizing and reducing uncertainty for low-risk systems, and there is a need to adapt these methods for risk-tolerant settings. Current uncertainty-based approaches include:

- Uncertainty-based multidisciplinary design optimization has been used to maximize performance under uncertainty; see Yao et al. (2011) for a review paper.
- Assessing performance under uncertainty using large, integrated models of space systems, e.g., the Gen-eralized Information Network Analysis (GINA) methodology developed by Shaw et al. (1999, 2001) or performance characterization of the JPL Skycrane for landing the Curiosity rover on Mars by White et al. (2012).
- Reducing the variance of a performance estimate for an existing design, as in Sondecker IV (2011), Stout (2015), or Sankararaman (2016).
- Designing systems that are robust to uncertainty. Masterson and Miller (2004) developed an approach for tailoring the design of space systems prior to launch to be robust to uncertainty, and to be able to tune out the remaining uncertainty on orbit.

The common theme in these methods is that uncertainty is not desirable, and therefore it must be characterized and reduced, which is appropriate for high-budget, low-risk systems. However, risk-tolerant platforms such as nanosatellites may be able to tolerate some performance variation if it enables the reduction of cost or improves manufacturability.

[3] 1064 nm, with data rates of 622 Mb per second.

[4] 1550 nm, with data rates of up to 100 Mbps, used as a reference in this paper.

2.2. Need for Uncertainty Quantification for Multidisciplinary Nanosatellite Models

Multidisciplinary nanosatellite system modeling has been used to integrate systems engineering and subsystems such as structures, thermal, optical, controls, and others, but it has not been combined with direct quantification of hardware-specific input uncertainties. The approach in this paper complements recent nanosatellite modeling efforts such as Model-Based Systems Engineering (MBSE) for test and verification activities (Bjorkman et al., 2012), MBSE for CubeSat operations simulations (Kaslow et al., 2014; Spangelo et al., 2013; Spangelo and Cutler, 2012; Spangelo et al., 2012), and the TeamXc software tool (Zarifian et al., 2015) by providing input distributions and a methodology for using them to design under uncertainty. Performance uncertainty quantification for nanosatellites has been limited to indirect methods, specifically, the use of expert elicitation (Babuscia and Cheung, 2013), and there remains a need to comprehensively estimate model input distributions based on first principles and experimental data. A direct input distribution characterization approach has been used for deep-space RF communications for interplanetary spacecraft (Cheung, 2010) but not for nanosatellites or lasercom. Using these distributions also requires a statistical modeling approach for simulating nanosatellite performance, which we address in this paper.

2.3. Lasercom Modeling

As a foundation for LUMOS, this section describes the state of the art in lasercom subsystem and end-to-end system modeling, and defines key terms. The literature has generally focused on subsystem modeling (e.g., theoretical analysis of spatial tracking performance to predict pointing losses (Win, 1989; Win and Chen, 1992)) or on large, deterministic models. Statistical link estimation has been used to assess the probability of closing a link under various atmospheric conditions for deep-space optical communication (Biswas and Piazzolla, 2003). The current study builds on this work by investigating how system design can be improved with a probabilistic approach, by developing a comprehensive, hardware-specific library of input distributions for the NODE space terminal (Clements et al., 2016) that can be generalized to other lasercom systems, and incorporating these distributions in an integrated, probabilistic system performance model.

2.3.1. End-to-End Lasercom System Modeling

Probabilistic lasercom models have been used for free space optical (FSO) ground network optimization to mitigate the effects of cloud cover. Alliss and Felton (2012) developed the Lasercom Network Optimization Tool (LNOT), which uses fractional cloud cover based on GOES data to estimate the cumulative probability distribution for the daily percent data transferred of a hypothetical mission that generates 12 Tb per day, with 2.3 Tb of on-board data storage, corresponding to 4.5 hours of acquisition time. The work of del Portillo et al. (2017) optimizes optical ground site selection for the metrics of availability, latency, and cost with variable cloud cover. The LUMOS approach aids in the design of space and ground terminals rather than selecting ground stations as in Alliss and Felton and del Portillo et al.'s work. It extends their probabilistic metrics to both space and ground terminal design and combines this with the cloud availability modeling approach of del Portillo et al.[5]

Probabilistic models are also used to assess lasercom designs. For example, Biswas and Piazzolla (2003) evaluated best, worst, and nominal data rates for the Mars Laser Communication Demonstration (MLCD) using input probability distributions including pointing error, atmospheric effects, and background radiance. In the LUMOS model, we extend this approach to estimate a probability distribution of a key performance metric, such as data volume delivered during a given time interval, instead of assessing best, worst, and nominal cases.

[5] The LUMOS model is modular, and could interface with an alternate cloud cover model to simulate ground station availability.

2.3.2. Lasercom Subsystem Modeling

Lasercom systems engineering focuses on decomposing the system into subsystems and modeling at lower levels, rather than building an end-to-end integrated system model. A summary of literature on lasercom subsystem modeling is shown in Table 1. We build on this existing work for the LUMOS input distribution library.

3. Case Study Implementation Details

The objective of the case study is to assess the performance and manufacturability improvements with the LUMOS approach, using both deterministic and probabilistic performance metrics as described in Section 3.2. We will assess the design performance using three approaches:

i. *Optimization with Worst-Case Inputs:* This approach optimizes for a deterministic performance metric; the average data volume per day under worst-case conditions. This reflects a traditional systems engineering approach.
ii. *Optimization with Input Distributions:* This approach, which reflects a hybrid probabilistic-traditional approach, replaces the inputs from Approach 1 with input distributions, but maximizes the same performance metric.
iii. *Optimization for a Probabilistic Metric:* This approach replaces the metric of maximizing data volume with mini-mizing the probability of failing a daily data volume requirement, and explores how much manufacturability can be improved with this approach. This reflects the new probabilistic approach.

This section describes the implementation of the LUMOS approach for nanosatellite lasercom design. We provide details of the metrics, the link modeling, and day-in-the-life simulation implementation of LUMOS for the case study.

3.1. Nanosatellite Lasercom Design Case Study Overview

We use the design of a communication system with the NODE lasercom architecture for a CubeSat generating large data volumes of up to 500 Gb/day, because, for example, the science payload is a hyperspectral imager, as illustrated in Figure 1. Hyperspectral imagers are of interest for CubeSat missions because of their use for missions such as hydrology, minerology, and agriculture monitoring (ESA, 2014). These payloads can produce large volumes of data, and even after compression, common CubeSat communication systems such as UHF or S-band limit the useful duty cycle of these instruments. NODE uses a

Table 1. Summary of Key Components, Design Parameters, and Subsystem Characterization*

Link Block	Key Components	Design Parameters	Previous Characterization
Space Terminal	Transmitter electronics, optics, a pointing control system, and mechanical support	Aperture diameter, which controls the width of the transmit beam, and pointing control	Pointing control variations have been demonstrated to create received power fluctuations, as in Kolev and Toyoshima (2017)
Channel	Clouds and atmospheric turbulence	Fried parameter (r_0), which measures atmospheric coherence length, and C_n, the atmospheric structure parameter (Andrews and Phillips, 2005)	Atmospheric attenuation and turbulence conditions have been characterized at a limited number of candidate ground station locations (Alliss and Felton, 2010; Nugent et al., 2013). Wilson et al. (2012) compares MODTRAN (a software tool that simulates optical transmission at a range of wavelengths) data with statistics of measurements at the Optical Communications Telescope Laboratory (OCTL) from 2006–2011. Alliss and Felton (2012) have extensively characterized cloud-related availability of different ground sites including OCTL.
Ground Terminal	Telescope, a detector to translate received photons into an electrical signal, and receiver electronics to process the signal	Ground station aperture and detector selection	Implementation losses, which capture difference in performance between theory and practice, of about 3 dB have been observed in the laboratory (Kingsbury, 2015, p. 89), but these may vary when transitioning from a prototype to a field unit.

*Further information on the key components can be found in Hemmati (2009).

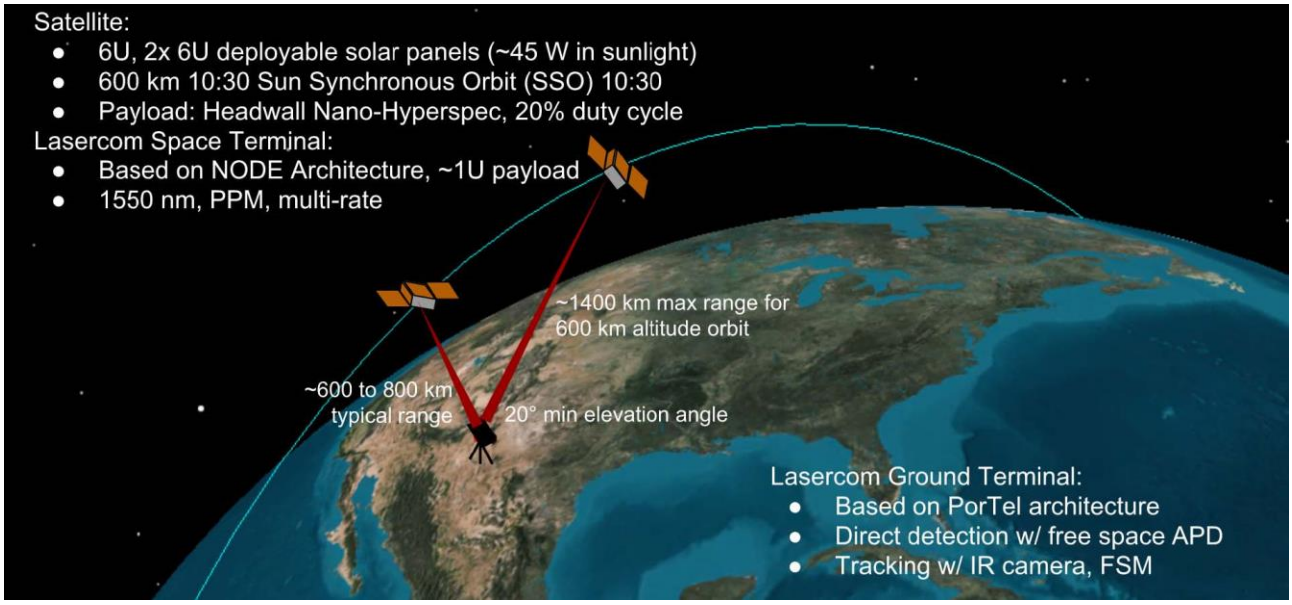

Figure 1. Overview of the mission and lasercom link for the LUMOS case study. A 6U CubeSat with two 6U deployable panels carries a hyperspectral imager in a 600 km Sun Synchronous Orbit (SSO). The NODE architecture is used for the lasercom downlink to a ground station with the PorTeL (Riesing et al., 2017) architecture. PorTeL has an Avalanche Photodiode (APD) receiver and a Fast Steering Mirror (FSM) for tracking.

direct detect Master Oscillator Power Amplifier (MOPA) transmitter to allow multi-rate communications with a fixed slotwidth by changing Pulse Position Modulation (PPM) order. A Fast Steering Mirror (FSM) system provides fine pointing to augment coarse body pointing. For the ground station network, we assumed one ground station is located at each of the BridgeSat network locations shown on the BridgeSat website (2018) as a representative geographically-distributed network, but any set of latitudes and longitudes could be used for ground sites.

3.2. Probabilistic Metrics

The use of statistical models enables the use of probabilistic metrics. As an alternative to the objective function of maximizing data volume, we assess the probability of reliably communicating a critical data volume, 500 Gb of data per day. Once designs that achieve this data volume requirement are identified, then the "acceptable" designs can be down-selected based on secondary metrics.

To estimate a critical data volume, we assume the imager operates at a 20% duty cycle. Because Earth-observing missions are often observing land mass, which makes up about 30% of the Earth's surface, and only 30% of land mass is cloud-free at any given moment (NASA, 2018), we use 20% duty cycle here as a conservative estimate (roughly double the average duty cycle per day). Operating the Nano-hyperspec (Headwall, 2018), which was proposed by Mandl et al. (2015) for a CubeSat hyperspectral imaging mission, at 10 frames per second for one day at 40% compression would produce 500 Gb of data per day.

We use as secondary metrics the aperture of the ground station receiver and beam width of the space terminal transmitter as proxies for cost and manufacturability. Systems that are more difficult to manufacture (less manufacturable) are more expensive to assemble, even if individual components are not expensive. Telescope cost scales with the diameter of the telescope (Lesh and Robinson, 1986), and it is cheaper to set up a smaller diameter ground station because of the smaller footprint. On the space terminal, smaller apertures mean larger beams, which means larger misalignments can be tolerated, translating to shorter integration time, improved manufacturability, and therefore lower cost, although with lower power efficiency.

3.3. Model Setup

LUMOS is a multidisciplinary model of a day in the life of a CubeSat, incorporating the disciplines of physics, optics, orbital dynamics, link analysis, and atmospheric dynamics. We model the required power using Gaussian statistics. Model validation using data from the Lunar Laser Communication Demonstration is described in the appendix, and further details can be found in Clements (2018).

The LUMOS model, illustrated in Figure 2, accepts bounds for each input variable listed in Table 2 and randomly generates a set of vectors of design inputs (called design vectors) to form the first population of the optimization. Each design vector is assessed through Monte Carlo analysis to determine either the average data volume per day in the deterministic metric cases and the probability of failing to meet a data volume requirement in the probabilistic metric case. The optimization algorithm then selects the highest-performing members of the population of design vectors and generates a new population. Then, these are assessed through Monte Carlo analysis, and the cycle is repeated until the optimization has completed twenty generations without further improvement.

The design optimization leverages the particle swarm and genetic algorithms from the MATLAB optimization toolbox (Mathworks, 2018). Heuristic algorithms were selected because they handle the discontinuities in performance that result from the constant slot width of the NODE architecture better than a gradient-based algorithm.[6] The input variables and bounds are given in Table 2. Particle Swarm was used for the single objective optimization cases of (i) Optimization with Worst-Case Inputs and (ii) Optimization with Input Distributions, and the multi-objective genetic algorithm was used for case (iii). A population of 100 was used for each generation of the genetic algorithm, and a Monte Carlo analysis with 1000 runs[7] of the constellation simulation was performed for each population member to estimate the expected performance of each design point.

The satellite day-in-the-life simulation estimates the data volume transferred by a nanosatellite lasercom system over three days,[8] and estimates an average daily data volume. The model calculates the data

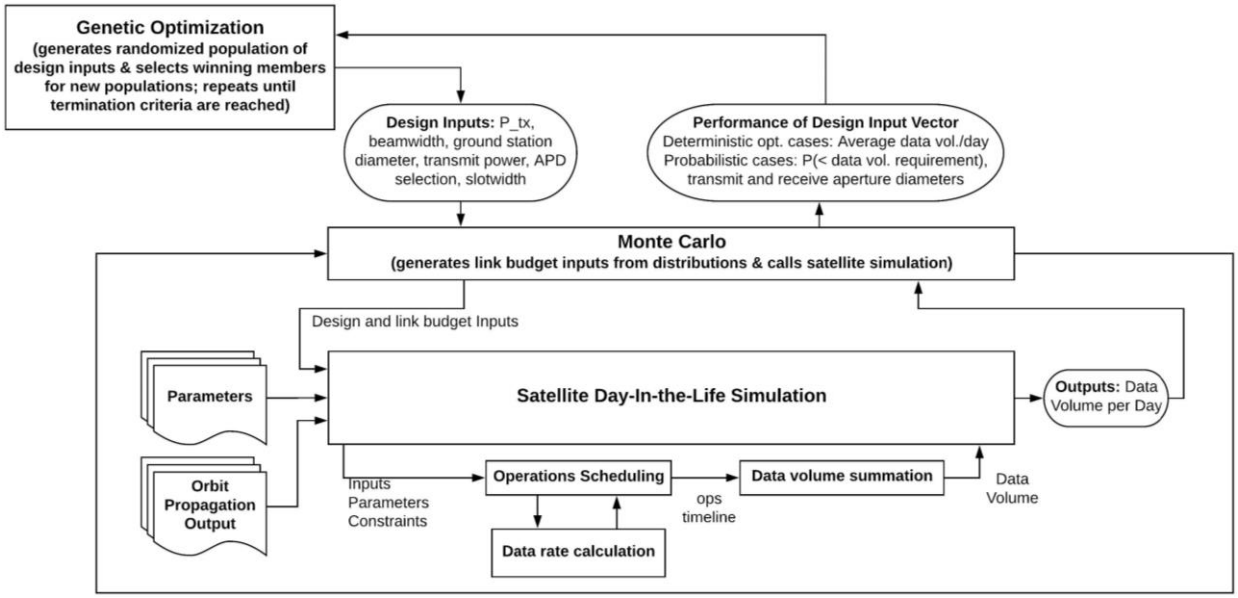

Figure 2. Analysis steps of the genetic optimization, Monte Carlo, and day-in-the-life simulations.

[6] Because the slot width is held constant, continuous changes in received power cause steps in data rate.

[7] The exact error bar depends on the inputs and system performance. For the design vectors used in the results section, 1000 runs is sufficient to estimate the average daily data volume to better than 3% with 95% confidence.

[8] Three days at 500 Gb per day would be equivalent to a maximum on-board storage of 1.5 Tb (less than 200 GB), which is consistent with the data storage capability of CubeSats.

Table 2. Bounds for the Input Variables for Optimization Studies

Ground station diameter	0.3 to 1 m	1 m is the common upper bound for lasercom ground stations. Below 30 cm, aperture averaging assumptions in the model are no longer valid. We assume a focal length of 8 times the diameter based on f-numbers for amateur telescopes.
Slot width	0.48 to 5.0 ns	The minimum slot width is based on the maximum APD bandwidth of all the APDs considered, 2.1 GHz, which works out to 0.476 ns. If a slot width is selected that is slower than the selected APD can achieve, it is adjusted to be the minimum slot width for that APD. From these slot widths we can estimate the minimum and maximum data rate; PPM-4 with 0.48 ns slot width corresponds to 760 Mbps, and PPM-512 with 5 ns slot width corresponds to 3.2 Mbps, accounting for header bits, inter-symbol guard time, and coding. The maximum is an order of magnitude larger than the minimum, and equal to that used by the NODE program.
Transmit Power	0.1 to 0.5 W	Up to about 0.5 W is reasonable for an EDFA that would fit in a 1-U lasercom transmitter.
Detector	1 to 12	List of 7 APD Photoreceivers from the Voxtel catalog (Voxtel, 2015), three Hamamatsu APDs (Hamamatsu, 2017), and two Princeton Lightwave Photorecievers (Princeton, 2017). If more transmit power is available, the selection of APDs could be re-examined, as additional margin could enable higher data rates if the receiver and system electronics could support it.
Half Power Beamwidth	0.1 to 2.0 mrad	2 mrad is relatively easy to achieve, as planned with NODE. The model is considered valid down to 0.1 mrad; beams smaller than this may have pointing losses not accounted for in this model.

rate for a given set of inputs and access conditions (time and range), and takes in access times and corresponding ranges from an open-source orbit simulation developed by A. Kennedy (Cahoy and Kennedy, 2017).[9] An achievable data rate is determined based on the range and other conditions for each timestep such as atmospheric loss. We note that while the model was built for the NODE program, it is modular, enabling easy adaptation to other architectures.

3.4. Link Budget and Input Distributions

The link budget is based on the link budget described in Clements (2018) for the NODE program. Representative links are shown in Table 3. Most of the inputs in this link budget are updated as input distributions, as shown in Table 4, or are used as design variables as described in Table 2. Note that the architecture is multi-rate using M-PPM; with fixed receiver sensitivity (fixed number of photons/bit or PPB required), the required receive power is reduced with the data rate for a fixed slot width. With an Mary multi-rate system the receiver sensitivity improves (i.e., fewer PPB are required) as M is increased and the rate is decreased.

Table 4 is based on distributions that follow those described in Clements (2018). Each run of the Monte Carlo analysis calculates transmitter optical loss, pointing loss, free space loss, atmospheric loss, receiver optical losses, etc. and calculates received power. The ratio of the resulting received power at the ground-based detector with the required power for a given data rate gives the margin, and the data rate is adjusted until the received power is greater than the required power.

4. Results

In this section, we compare the results from the LUMOS modeling approach with those obtained through more traditional satellite systems engineering approaches. First, (i) the traditional conservative approach of designing for worst-case inputs is compared

[9] The simulation uses the orbit propagation simulation "Attitude Propagator" (PROPAT) by Carrara (2015) combined with custom post-processing in MATLAB to determine access windows for downlink opportunities.

Table 3. Representative Link Budgets for Several Nanosatellite Downlink Cases*

Key Input Parameters	Link A	Link B	Link C	Link D	Units	Notes
Channel data rate	11	50	300	400	Mbps	
Information data rate	9.9	43	244	292	Mbps	Rates include scaling factors for error correction bits, header bits, etc.
Slot width	5.00	5.00	1.25	1.25	ns	
PPM order	128	16	8	4		
Average optical output power	0.20	0.20	0.50	0.50	W	
Laser Wavelength	1550	1550	1550	1550	nm	
Half-power beamwidth	1.33	1.33	0.500	0.200	mrad	
Receive Aperture diameter	30	100	30	100	cm	Bounds from Table 2
Link Budget Summary						
Laser avg. optical power	–7.0	–7.0	–3.0	–3.0	dBW	
Transmit optical losses	–1.5	–1.5	–1.5	–1.5	dB	
Transmit antenna gain	69.6	69.6	78.1	86.0	dBi	
Pointing loss	–3.0	–3.0	–3.0	–3.0	dB	Fixed for this representative link; in reality pointing error is independent of beamwidth so it would not always be 3 dB loss.
Path loss at 1000 km	–258.2	–258.2	–258.2	–258.2	dB	Note that path loss for 1400 km is about 3 dB greater
Atmospheric loss	–1.0	–1.0	–1.0	–1.0	dB	Representative value; can use MODTRAN to improve estimate
Receive antenna gain	115.7	126.1	115.7	126.1	dB	
Receive optics losses	–2.0	–2.0	–2.0	–2.0	dB	–1 dB for beamsplitter plus miscellaneous losses
Receiver Implementation loss	–3.0	–3.0	–3.0	–3.0	dB	Measured value from Kingsbury (2015)
Signal power at detector	–87.3	–77.0	–75.0	–56.6	dBW	
Signal power req'd, BER=1e–4	–93.2	–84.2	–78.2	–73.0	dBW	Includes implementation loss
Receiver Sensitivity	339	593	394	978	Photons per bit	Calculated based on required power & data rate
Margin at 1000 km	5.8	7.2	3.2	16	dB	Typical range
Margin at 1400 km	2.8	4.2	0.2	13	dB	Maximum range includes additional 3 dB in path loss. (Atmospheric loss was held at –1.0 dB as a representative value, but is adjusted for elevation angle in the LUMOS code.)

*Links A and B have 0.2 W transmit power and 1.33 mrad half power beam width, while Links C and D have 0.5 W transmit power and 500 and 200 μrad half power beam width, respectively.

with (ii) the approach of designing with input distributions. Then we compare the designs resulting from (ii) traditional metrics of maximizing a function (in this case data volume) versus (iii) a probabilistic metric (in this case the probability of achieving 500 Gb per day).

4.1. Optimization under Worst-Case Assumptions vs. Optimization under Uncertainty

We first compare the results of (i) optimization under worst-case assumptions for the performance metric of average data volume downlinked per day with the results of (ii) optimization under uncertainty. Because formal cost-estimating relationships have not been defined for nanosatellite lasercom systems, we use ground station diameter and half-power beam width as proxies for cost. As will be discussed further in Section 4.3, ground station cost scales polynomially with ground station diameter, and larger transmit beams reduce the on-board alignment requirements.

As shown in Figure 3, optimization under worst-case inputs drives selection of designs with larger beam widths (0.23 mrad vs. 0.19 mrad), while both have large receiver apertures (93 cm and 91 cm). While the two designs have similar apertures, the optimization under worst-case inputs uses a larger APD with lower bandwidth re-sulting in a longer slot width and lower data rate (see Table 5 for the full design vectors). These conservative design decisions limit data volumes to about 1.7 Tb per day for a satellite in an LEO sun-synchronous orbit, while optimization under uncertainty leads to designs with expected data volumes of about 2.2 Tb per day.

Table 4. Input Distributions for Monte Carlo Analysis*

Variable	Distribution	Val. for Worst-case Opt.	Rationale
Pointing error	N(0, 0.025) + U(−0.092, 0.092) mrad	0.117 mrad	Sum of errors from pointing budget and thermoelastic misalignments
HPBW	Uniform distribution, ± 1% of beam-width	beamwidth	Per collimator datasheet (Thorlabs, 2010), collimation at room temp. is accurate to 1%.
Tx optical losses	N(−1.5, .5) dB	–3.0 dB	Assumes 0.1 dB per splice with 0.5 dB standard deviation from thermal-induced output variations of electro-optical components.
Extinction Ratio (ER)	U(6.31×10^{-5}, 1.58×10^{-4}) (–42.0 dB to –38.0 dB)	–38.0 dB	Reported in Kingsbury (Kingsbury, 2015, pp. 82–87) that ER varied between –38 and –42 dB
Implementation Loss	U(6.30957 × 10−5,0.000158) dB (-3.5 to -2.5 dB)	–3.5 dB	Measured by Kingsbury (Kingsbury, 2015, p. 89) as –2.4 to 3.0 dB; added half a dB for further implementation loss at system integration level.
Receiver Optical Loss	U(0.35, 0.50) (transmission) (−4.55 dB to −3.00 dB)	-4.55 dB	Optical losses typically a few dB
Ground Station Availability	20% to 84%	20% to 84%	Analysis performed by another MIT graduate student, I. del Portillo Barrios using data from MODIS (del Portillo Barrios, 2016)
Atmospheric Loss at zenith	U(0.82, 0.99) (transmission) (−0.86 dB to − 0.044 dB)	–0.86 dB	MODTRAN simulation
Fried Parameter at zenith, r_0	U(0.06, 0.43)cm	12 cm	Alliss and Felton (2010)

*The distributions are uniform in scalar units rather than decibel units. Further discussion of each input distribution is in the Appendix.

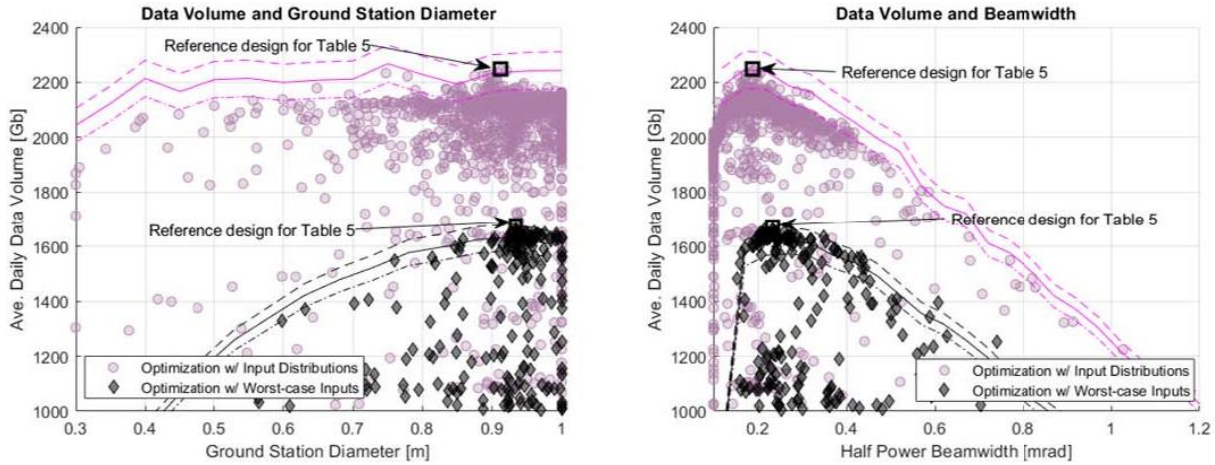

Figure 3. A comparison of (i) optimization under worst-case assumptions (black) and (ii) optimization under uncertainty (purple) shows that worst-case optimization leads to more conservative systems with lower data volume. Each point represents the mean of a 1000-run Monte Carlo with an individual design vector. To show the dependence of each design vector on ground station diameter and beam width as well as the number of runs, we show curves for the mean and +/-3% of the mean for each of the reference design vectors with 1000 Monte Carlo runs. A total of 1000 runs was selected to achieve results within 3% of the mean with 95% confidence.

4.2. Optimizing Data Volume vs. Optimizing for Manufacturability Under Uncertainty

While optimization under uncertainty can outperform optimization with worst-case assumptions for deterministic metrics, here we investigate whether a probabilistic metric, i.e., the probability of achieving a mission-specific data volume requirement (discussed in Section 3.2), can lead to more practical systems for mission-specific needs. Maximizing average data volume per day may lead to average data volumes that are much higher than required for a given mission.

In case (iii), we minimize the probability of failing to meet a requirement while maximizing manufacturability. In Figure 4, we show the results for case (iii) with both the probability of downlinking less than 500

Table 5. List of the Winning Design Vectors for Each Design Approach*

Approach	Metric	Detector	Slot Width [ns]	Rx Diam. [cm]	Tx Power [W]	HPBW [mrad]	Data Vol/day [Gb/day]	P(<500 Gb/day)	P(<250 Gb/day)
Traditional (worst-case)	Max(Data Vol/Day)	7	0.67	93	0.50	0.23	1650	0%	0%
Optimization w/ dist	Max(Data Vol/Day)	5	0.48	91	0.50	0.19	2200	0%	0%
Opt. for Prob. Metric	Min(P(<500Gb/day))	7	1.06	37	0.27	0.22	900	6%	0%
De-scoped Prob. Metric	Min(P(<250Gb/day))	7	1.06	30	0.27	0.42	450	70%	5%

*The probability estimate is based on the fraction of the 1000 Monte Carlo data volume results that are less than the 500 Gb/day requirement. APD 5 has a diameter of 75 microns while APD 7 has a diameter of 300 microns so seeing loss is larger for APD 5 and would require more received power to achieve the same data rate, but APD 5 is capable of higher bandwidth. (Seeing loss, caused by turbulence-induced increases in spot size relative to receiver diameter, will be worse for smaller receiver diameters for a given expanded spot size.) Note that relaxing from 0% probability of not meeting the 500 Gb/day requirement in the Optimization with distributions case to 6% in the Optimization for the Probabilistic Metric allows over a factor of 2 decrease in ground station diameter.

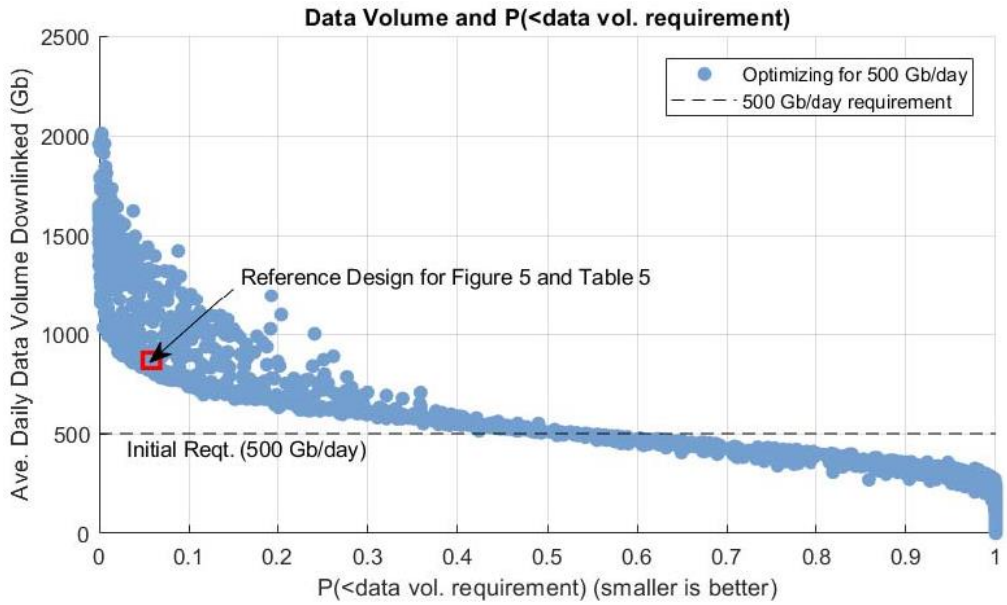

Figure 4. Comparison of the metrics of maximizing data volume and minimizing the probability of failing to achieve a required data volume, with optimization results for the probabilistic metric. Higher average data volumes indicate lower probabilities of failures, but with diminishing returns for the highest data volumes.

Gb per day and the mean daily data volume of each design to show how the new, probabilistic metric relates to the deterministic metric. The probabilistic metric trends with average daily data volume, but with diminishing returns on increasing data volumes. We identified the designs that have less than a 10% probability of failure and then selected the design with the smallest ground station (0.37 m) paired with a relatively large beam (0.22 mrad) and low transmit power (0.27 W), as indicated with the red box.

For a resource-constrained program, it may be desirable to explore de-scoping a requirement to improve manufacturability even further than the design result of (iii). To illustrate the impact of changing design inputs around the values at the point of diminishing returns, Figure 5 shows performance results with varied ground station diameter and beamwidth using the design vector identified in Figure 4. Unlike with a deterministic model, we can compare the probability of meeting the original and relaxed requirements for each set of inputs. As shown in Figure 5, the probability of failing to achieve each performance metric goes up with larger beamwidths and smaller ground stations. A design with a large beam-width and small ground station is more likely to meet the 250 Gb/day

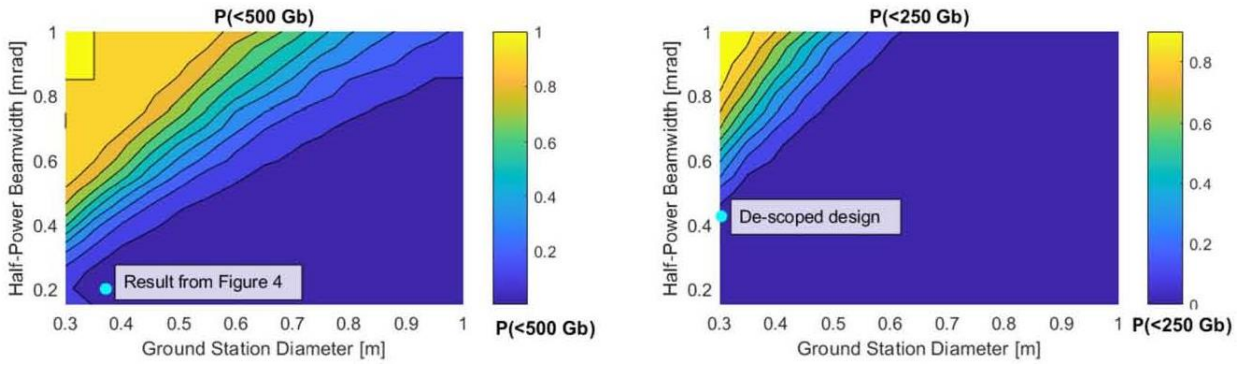

Figure 5. Parametric study of the changes in the probability of failing to achieve a daily data volume requirement based on changes in ground station diameter and half-power beam width. The left figure gives the probability of achieving less than 500 Gb per day (indicated by the colormap), and the right figure gives the probability of achieving less than 250 Gb per day. The design vector from the reference design from Figure 4 is used for the APD, power, and slot width. The design point with the ground station and beam width of the reference design from Figure 4 is circled in cyan, with a 37 cm ground station diameter, a 0.22 mrad beam width, and a probability of failing the 500 Gb/day requirement (left figure) of 6%. By reducing the requirement to 250 Gb/day (right figure), the ground station diameter is reduced to 30 cm, and the beam width can be expanded to 0.42 mrad. Note that the pointing error increases faster than the improved transmit gain when beam widths are reduced below about 0.2 mrad for this system, causing the artifact in the 500 Gb figure.

requirement than the 500 Gb/day requirement. The implications of this difference on cost and manufacturability are discussed in Section 4.3.

4.3. Discussion

By comparing the optimal designs from each approach, we can understand the impacts of the different designs on the practicality of each system. The input vector and performance of each design are listed in Table 5. We first discuss the implications of the different ground station diameters, beam widths, and transmit powers of the results from the optimization under (i) worst-case assumptions, (ii) optimization under uncertainty, and (iii) optimization for P(<500 Gb) cases. We then discuss the implications of relaxing the probabilistic metric to P(<250 Gb) per day.

4.3.1. Receiver Aperture

The receiver apertures for (i) worst-case assumptions and (ii) optimization under uncertainty are relatively large, at 93 cm and 91 cm respectively. In contrast, the probabilistic approach allowed the optimization routine to back off on ground station diameter, enabling a 37 cm ground station.

The smaller ground station diameter is important for reasons of cost and practicality. Optical communication ground station cost is highly dependent on diameter of the telescope (Lesh and Robinson, 1986). The 37 cm is within the range of commercially available amateur astronomy telescopes. This costs about $5k for Meade or Celestron telescopes (Celestron, 2018; Meade, 2018), up to $38k for the smallest (a 40 cm) observatory-class telescope system (PlaneWave, 2018).[10] In contrast, a 1 m observatory-class telescope is $650k (PlaneWave, 2018), and might require more highly skilled personnel to assemble and operate.

4.3.2. Transmitter Beam width and Power

Beam width can affect the cost of the system, as a larger beam reduces the tight alignment and pointing requirements on the space terminal. (It also reduces the size of the aperture required, but even the aperture for 0.19 mrad—about 15 mm, allowing for an aperture slightly larger than the diffraction limit—is not difficult to fit on a CubeSat.) Increasing the size of the beam increases the necessary output power for a required received power. Higher transmit power requires

[10] The observatory-class system cost includes the cost of a mount, while the other telescope costs do not include the mount.

a larger transmitter fiber amplifier. Therefore, the designer must evaluate the cost of alignment and pointing compared with the cost of additional SWaP and thermal control for higher output power in making their decision. Note that higher transmit power would enable greater link margin, and the selection of receivers could be re-examined to see if faster detectors could be used to enable a higher data rate with the extra link margin.

4.3.3. Risk in System Design Decisions

While the P(<500 Gb downlink per day) metric resulted in a more manufacturable design than the cases with deterministic metrics, mission architects may still wish to explore ways to further reduce cost, and improve ground station portability or other metrics by relaxing the requirements. For this hypothetical hyperspectral imaging mission, 500 Gb was a conservative upper bound of payload data production, and diminishing returns may be reached after a lower daily downlink data volume. To test this, we examine the impact of lowering the original requirement to 250 Gb per day.

For the reference design in Table 5, we selected a design that had a larger beam width of 0.42 mrad and a smaller receiver diameter of 30 cm, to illustrate how relaxing the requirement can allow for designs with very different inputs. Even with the relaxed requirement, the design may still achieve the original performance requirements on average; in Table 5 we see the design for the 250 Gb per day requirement still exceeds 500 Gb per day in 34% of cases.

5. Conclusion

This paper describes the implementation of a modeling framework called LUMOS, which leverages statistical components to enhance conventional systems engineering capabilities, and facilitates the decision-making process for risk-tolerant systems with uncertainties such as nanosatellite-based laser communication platforms. Relative to traditional approaches, LUMOS yields more manufacturable designs and lower-cost architectures.

To evaluate the advantages of using the LUMOS methodology over traditional design-optimization techniques, we performed three case studies: (i) the "traditional" case, using deterministic metrics for maximizing data volume and worst-case assumptions for inputs; (ii) using input distributions and the same deterministic metric; and (iii) using input distributions and a probability metric for achieving a specific data volume requirement while maximizing manufacturability. Some noteworthy benefits include: 1) a 33% improvement in average downlink daily data volume over optimization with worst-case assumptions for inputs when using the traditional metric of maximizing data volume; and 2) a significantly smaller, more manufacturable system (37 cm versus 91 cm diameter ground station) that can achieve a high probability (>90%) of meeting the design requirement. Furthermore, the LUMOS approach provides a means of more accurately assessing the impact of design trades and margin on probable system cost and performance in the presence of uncertainties.

While this work demonstrates the utility of the LUMOS approach for nanosatellite-based laser communication systems, it could be extended to other mission areas. For example, future work could investigate the impact of atmospheric input distributions on LIDAR, weather sensing radiometry, imaging missions, or other applications that are sensitive to atmospheric channel transmission.

Appendix

Spacecraft Assumptions

This section summarizes the assumptions about spacecraft power capabilities, and we refer the reader to Clements (2018) for further details. We use a 6U CubeSat to be consistent with Mandl et al. (2015), and we placed it in a 600 km sun-synchronous orbit to achieve constant illumination during Earth-imaging operations.

Power Consumption: The spacecraft consumes approximately 10 W orbit average power during sunlight nominal operations and an additional 5 W during eclipse for heaters. The 10 W orbit average power in-

cludes a duty-cycled 13 W payload, equal to the maximum power of the Nano-Hyperspec (Headwall, 2018), operated at a 20% duty cycle. We assume the transmitter consumes 2 W for electronics and that the EDFA is 5% efficient,[11] such that the total consumed power of the transmitter is 2 + 20 × Ptx.

Power Generation and Storage: We assume the spacecraft is equipped with state-of-the-art solar panels and batteries. State-of-the-art small satellite solar panels typically achieve 30% efficiency, and batteries achieve about 150 W-hr/kg energy density (Frost et al., 2015). We assume the cells have a 60% packing efficiency, and that two 6U panels can deploy, generating 45 W of power in sunlight. We assume a battery of 0.33 kg, giving 50 W-hrs of storage.

Ground Station Assumptions

Telescope mounts often have an exclusion angle, usually a zenith exclusion angle, through which they cannot slew fast enough to track low Earth orbit (LEO) objects. At this time, the PorTeL system has a 20 degree zenith exclusion angle constraint, which we use in the LUMOS model, although improvements are underway.

We assume a fixed ground station telescope focal ratio of 8 to be consistent with common amateur telescopes, which have focal ratios between 6 and 10. PlaneWave telescopes have focal ratios of 6 to 6.8 (PlaneWave, 2018), Celestron has 10 to 11 (Celestron, 2018), and Mead has a focal ratio of 8 (Meade, 2018).

Input Distribution Details

This section contains further discussion of the rationales for each of the input distributions in Table 4.

The shapes of the distributions are based on the specifics of the uncertainty surrounding the input. For inputs for which only the bounds are known, a uniform distribution is used as this is the maximum entropy distribution. For inputs that are sums of other many other inputs (such as misalignment errors or optical losses) a Gaussian distribution is used. Models based on empirical data, such as cloud cover variation, provide the shape of the distribution when enough information is available.

The way the parameters of the distribution are determined is specific to each distribution. For example, the bounds of the beam width are based on the data sheet for the type of collimator considered in this study. The pointing error variance is based on a traditional pointing error budget, in which misalignments are estimated based on part tolerances, control error, and estimation error. For further information, see Clements (2018), Chapter 3, pp. 53–61.

Space Terminal Losses

We assume a uniform distribution of ± 1% on the beam width of a given design because the data sheet for the NODE collimator lists a 1% tolerance (Thorlabs, 2010).

Transmitter optical losses are assumed to be Gaussian (in dB) because the total optical loss is the sum of smaller losses. Optical communication systems are connected internally with fiber optics. Splices are typically 0.01 dB of loss for multimode fiber (Optics, 2018), but the total number of splices is uncertain. NODE has at least two splices, but typically additional splices are included from rework and fiber service loops, so the expected number of splices is 5 to 10. Additional losses will occur from absorption at each free space optical surface.

The pointing error combines three sources of error: control error, bias from point-ahead error (error induced by the movement of the satellite during the time it takes light to travel between the space terminal and

[11] Electrical-to-optical (E/O) EDFA power efficiency is dependent on the design, the operational environment (e.g., input and output power levels, temperature range, etc.), and the amount of electronic control that is included in the efficiency calculation (Caplan, 2007; Desurvire, 1994). In practice, EDFA E/O efficiency can range from 3% for low-power 200 mW commercial-off-the-shelf EDFAs – where power efficiency was not a design driver (see e.g., Kingsbury et al. (2015)), to 13% efficiency for 10 W-class EDFAs designed for power-efficient space-based operation (Wysocki et al., 2006). The 5% estimate used for the low-power EDFAs considered here is a conservative lower-bound estimate of efficiency that can be obtained when power is an important design parameter.

the ground station; see Winick (1986) for an illustration), and thermo-elastic-induced error. The control error is estimated to be 75 μrad, 3-σ (Clements et al., 2017).[12] The point-ahead error is calculated at each timestep based on the elevation angle, and the maximum point-ahead angle for a 600 km satellite is 50 μrad. The maximum thermo-elastic misalignment is 92 μrad based on a thermal simulation of NODE and the coefficient of thermal expansion of the aluminum frame and lens assembly. The control error has a Gaussian distribution, but the point-ahead angle and thermoelastic misalignments do not, so these are added instead of Root-Sum-Squared (RSS).

Channel Losses

We bound channel-related losses using MODTRAN analysis and published test data and assume uniform distributions between these bounds, as this is the maximum entropy distribution when only bounds are known. This provides a conservative estimate for each channel-related loss. Sensitivity analysis is used to identify input distributions that are driving the design, so that they can be refined if that would affect the design outcome.

The biggest channel effect for laser communications is cloud cover-induced unavailability. We used MODIS data from the Terra and Aqua instruments (Hubanks et al., 2008) to determine the average fraction of the time each ground station was cloudy. We then used these cloud fractions as an input to a Markov Chain Monte Carlo model to simulate the variation in cloud cover over time based on the approach described in del Portillo et al. (2017). The details of the Markov Chain Monte Carlo model are described in Clements (2018).

Atmospheric loss is affected by the local visibility conditions of the ground station. We use MODTRAN to estimate the transmission under various conditions, and the input distribution is based on the bounding cases (Urban with 5 km visibility and Desert Extinction conditions) as shown in Figure 6. Note that cloud cover is treated as a separate access window constraint, so the atmospheric loss applies even when there are no clouds.

We estimate a range of values for the Fried parameter based on measurements of diurnal Fried parameter variations for four sites in Alliss and Felton (2010). In this work, we use the r0 values from Alliss and Felton for Dryden to be conservative, as this site had the lowest seeing out of the four sites characterized in that paper. (While nanosatellites could tolerate a reduced level of conservatism relative to large spacecraft programs, it is unlikely that all nine ground station sites would have exceptionally good seeing conditions.) We assume a 20 degree minimum elevation angle; below this, weak fluctuation theory does not hold (Andrews and Phillips, 2005) and seeing calculations may be inaccurate. Note that the lower bound on the Fried parameter distribution is smaller than the value canonically used for the deterministic case; for this input a conservative, but not an absolute worst-case, scenario is used (Biswas and Piazzolla, 2003).

Ground Station Losses

Receiver optical loss is modeled as a uniform distribution of optical transmission from 0.35 to 0.5. While the transmitter loss is a sum of an uncertain number several smaller losses, with several of the losses varying in-dependently (different manufacturers for several of the free-space optics), the primary uncertainty in the ground telescope optical loss is the coating used on the large optical surfaces. For example, Celestron uses the Starbrite optical coating on the window and mirrors, and this coating is not characterized out to 1.5 micron wavelengths. Because there is one uncertainty factor dominating the loss, and the factor does not vary independently with the losses on each surface, we treat this as a uniform distribution. A beam splitter diverts half the light for pointing control, so the total optical throughput is half, at best.

We note that other lasercom ground station architectures may have additional types of losses that are

[12] Jitter for CubeSats with state of the art pointing control systems is better than 1 arcsecond (Frost et al., 2015), so jitter is neglected in this work.

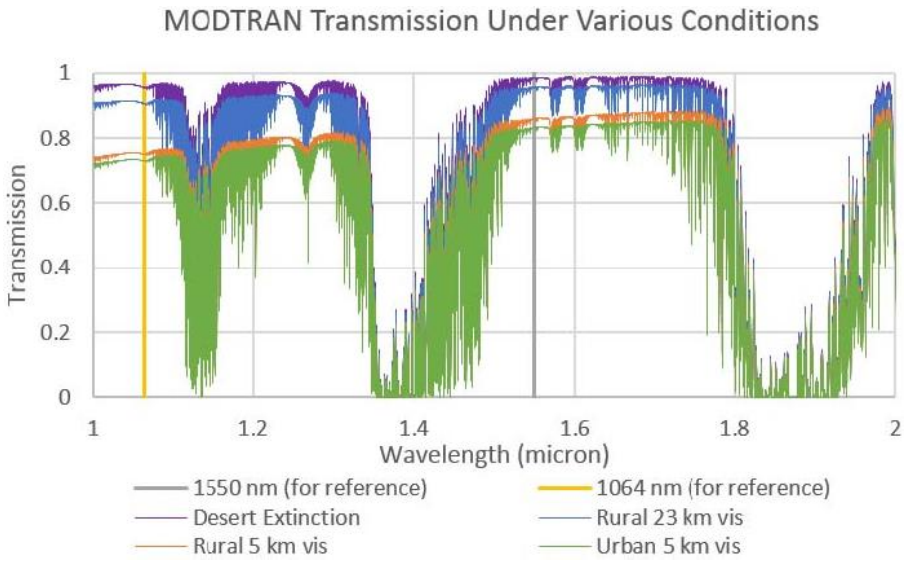

Figure 6. Optical transmission for 1 to 2 micron wavelengths under several environmental conditions (desert, rural with 5 and 23 km visibility, and urban with 5 km visibility). 1550 nm and 1064 nm are labeled for reference.

not yet accounted for in our model: pointing error; additional variable losses for an adaptive optics system; and variable detector noise due to temperature, to name a few. The NODE architecture of using relatively large receivers, with APDs up to 200 microns in diameter, combined with a robust tip/tilt control system reduces the need for more extensive adaptive optics. The APDs used by NODE do not have to be cooled, so detector temperature does not have to be modeled the way it would be for more sensitive, cooled detectors.

Other Operational Considerations

Lasercom operations can be limited by additional operational considerations, such as FAA aviation safety constraints, Laser Clearinghouse constraints, solar exclusion angle of the ground telescope, and max zenith angle of the telescope mount.

Laser operations that might affect aircraft are regulated, either by the FAA in laser-free flight zones around airports or by the laser safety office of the sponsoring agency. This is especially relevant for laser communication systems that have an uplink laser beacon or transmission, which could be non-eye-safe at low altitudes, although this could be mitigated by eye-safe LED beacons (Figura et al., 2018). The LLCD program estimated that for most passes, airplanes only restricted operations up to 10% of the time, but on rare occasions up to 70% of the pass could be affected (Biswas et al., 2012).

Similar to the aviation safety regulations, satellite safety also constrains laser operations. The eye-safe LED beacon would be too dim to affect satellites, but the downlink could affect satellites in the path of the beam. While the downlink schedule should be coordinated with Laser Clearinghouse for links conducted in the United States, in practice, only links that would be within 2.5◦ of other satellites are restricted (Edwards et al., 2016), and CubeSat orbits are so low (usually below 600 km) that such passes are infrequent.

Ground telescopes may be unable to tolerate the sun in or close to the field of view of the telescope due to background light, thermal constraints, detector damage concerns, or optics damage concerns, and this can limit the downlink opportunities. However, the fraction of the time that a satellite would pass between the ground station and the sun is small. The exact solar exclusion angle has not been assessed for the PorTeL system, but typical angles are about 8 degrees for other optical ground stations Biswas et al. (2014). Incorporating this constraint into the zenith exclusion angle model in STK gives a total of 3% reduction in access time with the combined zenith and solar constraints.

Comments on Monte Carlo Convergence

To illustrate the convergence of the Monte Carlo simulation, Figure 7 shows the mean data volume per day for the case (ii) design vector, estimated from 1 to 2000 Monte Carlo runs.

Comments on Model Verification

To verify that the model provides accurate results, it was used to simulate downlinks from LLCD to the Optical Communications Telescope Laboratory as published in Biswas et al. (2014). The majority of the cases resulted in received power between 50 and 200 pW, which is consistent with the results from Biswas et al., in which all of the received power fell between 40 and 160 pW. The SnSPDs can saturate at 160 pW, so the measured received power did not exceed this value. When comparing the results pass-by-pass, we found that 13 of the 19 passes resulted in measured received power that was within one standard deviation of the mean as predicted by LUMOS. All of the received power was within two standard deviations as predicted by LUMOS for each pass.

Acknowledgments

This research was funded by the MIT Lincoln Laboratory Lincoln Scholars Program. We would like to thank Andrew Kennedy and Hyosang Yoon, who helped in building the satellite day-in-the-life model, and Inigo del Portillo Barrios, who built the cloud cover model. We thank everyone who provided input and feedback on this paper, including Abi Biswas for information on interpreting the LLCD data for model validation, Raichelle Aniceto for EDFA and splicer information, Kathleen Riesing for ground station tracking and pointing control information, and Michael Shatz for general paper feedback.

DISTRIBUTION STATEMENT A: Approved for public release: distribution unlimited.

This material is based upon work supported under Air Force Contract No. FA8721-05-C-0002 and/or FA8702-15-D-0001. Any opinions, findings, conclusions, or recommendations expressed in this material are those of the author(s) and do not necessarily reflect the views of the US Air Force.

References

Alexander, S. B. (1997): *Optical Communication Receiver Design*, SPIE Optical Engineering Press: Bellingham, WA.

Alliss, R. J. and Felton, B. D. (2010): Improved Climatological Characterization of Optical Turbulence for Space Optical Imaging and Communications, in *Proc. Advanced Maui Optical and Space Surveillance Technologies Conf.*, Maui, HI, Sept. 14–17. Available online at: http://amostech.

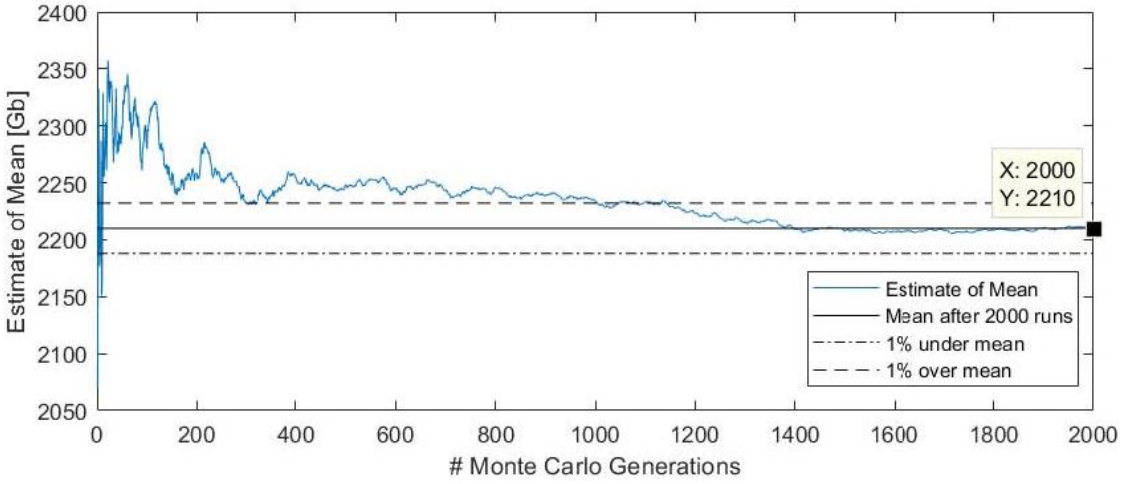

Figure 7. Illustration of convergence for case (ii) (optimization for maximizing data volume under uncertainty). 1000 runs is sufficient to estimate the mean to within about 1% for this design.

com/TechnicalPapers/2010/Adaptive_Optics_Imaging/Alliss.pdf (Accessed May 4, 2019).

Alliss, R. J. and Felton, B. D. (2012): The Mitigation of Cloud Impacts on Free-Space Optical Communications, in *Atmospheric Propagation IX*. Available online at: http://dx.doi.org/10.1117/12.918403 (Accessed May 4, 2019).

Andrews, L. C. and Phillips, R. L. (2005): *Laser Beam Propagation through Random Media*, Vol. 1, Bellingham, WA: SPIE Press.

Babuscia, A. and Cheung, K. M. (2013): Statistical Risk Estimation for Communication System Design. *Systems J., IEEE*, Vol. 7 (1), pp. 125–136.

Biswas, A. et al. (2014): LLCD Operations Using the Optical Communications Telescope Laboratory (OCTL), in *Free-Space Laser Communication and Atmospheric Propagation XXVI*. Available online at: http://dx.doi.org/10.1117/12.2044087 (Accessed May 4, 2019).

Biswas, A. and Piazzolla, S. (2003): Deep-Space Optical Communications Downlink Budget from Mars: System Parameters, *Inter-Planetary Network Prog. Rept.*, Vol. 42–154, Aug. 15. Available online at: https://tmo.jpl.nasa.gov/progress_report/42-154/154K.pdf (Accessed May 4, 2019).

Biswas, A. et al. (2012): OCTL Laser Beam Transmission Interruptions Due to Aircraft and Predictive Avoidance, *Inter-Planetary Network Prog. Rept.*, Vol. 42–191, Nov. 15. Available online at: https://ipnpr.jpl.nasa.gov/progress_report/42-191/191B.pdf (Accessed May 4, 2019).

Bjorkman, E. A., Sarkani, S., and Mazzuchi, T. A. (2012): Using Model-Based Systems Engineering as a Framework for Improving Test and Evaluation Activities, *Systems Engineering*, Vol. 16, No. 3., Jul. 29, 2013. Available online at: https://doi.org/10.1002/sys.21241 (Accessed May 4, 2019).

Boroson, D. M. et al. (2014): Overview and Results of the Lunar Laser Communication Demonstration, in *Free-Space Laser Communication and Atmospheric Propagation XXVI*. Available online at: http://dx.doi.org/10.1117.12.2045508 (Accessed May 4, 2019).

BridgeSat (2018): GLOBAL GROUND STATION NETWORK. Available online at: http://www.bridgesatinc.com/products/#ground (Accessed Apr. 6, 2018).

Buchen, E. (2014): SpaceWorks' 2014 Nano/Microsatellite Market Assessment, in *Proc. 28th Ann. AIAA/USU Conf. on Small Satellites*, Logan UT, Paper No. SSC14-I-3. Available online at: https://digitalcommons.usu.edu/cgi/viewcontent.cgi?article=3018&context=smallsat (Accessed May 4, 2019).

Cahoy, K. and Kennedy, A. K. (2017): Initial Results From ACCESS: An Autonomous CubeSat Constellation Scheduling System for Earth Observation, in *Proc. 31st AIAA/USU Conf. on Small Satellites*, Logan, UT, Paper No. SSC14-I-3. Available online at: https://digitalcommons.usu.edu/cgi/viewcontent.cgi?article=3629&context=smallsat (Accessed May 4, 2019).

Caplan, D. O. (2007): Laser Communication Transmitter and Receiver Design. *J. of Optical and Fiber Communications Repts.*, Vol. 4 (4–5), pp. 225–362.

Carrara, V. (2015): An Open Source Satellite Attitude and Orbit Simulator Toolbox for Matlab, in *Proc. XVII Int. Symp. on Dynamic Problems of Mechanics*, Natal, Brazil. Feb. 22–27.

Celestron (2018): Available online at: https://www.celestron.com/collections/telescopes (Accessed Mar. 22, 2018).

Cheung, K. M. (2010): Statistical Link Analysis - A Risk Analysis Perspective. *Inter-planetary Network Directorate Prog. Rept.*, Vol. 42 (183), Nov. 15.

Clements, E. et al. (2016): Nanosatellite Optical Downlink Experiment: Design, Simulation, and Prototyping. *Optical Engineering*, Vol. 55 (11), Sept. 13, p. 111,610.

Clements, E. et al. (2017): Integration and Testing of the Nanosatellite Optical Downlink Experiment, presented at the *31st Ann. AIAA/USU Conf. on Small Satellites*, Logan, UT. Available online at: https://digitalcommons.usu.edu/smallsat/2017/all2017/11/ (Accessed May 4, 2019).

Clements, E. B. (2018): Probabilistic Methods for Systems Engineering with Application to Nanosatellite Laser Communication, PhD thesis, Massachusetts Institute of Technology, Cambridge, MA.

Crabb, J. R. et al. (2019): Laser Transmitter for CubeSat-Class Applications, in *Free-Space Laser Communications XXXI*. Available online at: https://doi.org/10.1117/12.2506967 (Accessed May 4, 2019).

De Neufville, R. et al. (2004): Uncertainty Management for Engineering Systems Planning and Design, in *Proc. Engineering Systems Symp., Massachusetts Institute of Technology, Cambridge, MA*, Mar. 29–31.

del Portillo, I. et al. (2017): Optimal Location of Optical Ground Stations to Serve LEO Spacecraft, in *Proc. Aerospace Conf., 2017 IEEE*, Big Sky, MT, Mar. 4–11. Available online at: http://systemarchitect.mit.edu/docs/delportillo17a.pdf (Accessed May 4, 2019).

Desurvire, E. (1994): *Erbium-Doped Fiber Amplifiers: Principles and Applications*. New York, NY: Wiley and Sons.

Edwards, B. L., Lafon, R. E., and Luzhansky, E. Y. (2016): Operational Impacts of the US Federal Aviation Administration and the US Laser Clearinghouse on An Optical Communications Earth Relay, in *Proc. Aerospace Conf., 2016 IEEE*, Big Sky, MT, Mar. 5–12. Available online at: https://doi.org/10.1109/AERO.2016.7500534 (Accessed May 4, 2019).

ESA (2014): Hyperspectral Imaging By CubeSat On The Way. Available online at: http://www.esa.int/Our_Activities/Space_Engineering_Technology/Hyperspectral_imaging_by_CubeSat_on_the_way (Accessed Aug. 12, 2018).

Figura, J. et al. (2018): Initial Demonstration of An Uplink LED Beacon to a Low Earth Orbiting CubeSat: Tracking, Telemetry, and Communications (TT&C). *J. Small Satellites*, Vol. 7 (2), pp. 719–732.

Frost, C. et al. (2015): Small Spacecraft Technology State of the Art, *NASA Tech. Rept. TP-2015-216648/REV1, NASA Ames Research Center*.

Fuchs, C. et al. (2019): Update on DLR's OSIRIS Program and First Results of OSIRISv1 on Flying Laptop, in *Free-Space Laser Communication and Atmospheric Propagation XXXI*. Available online at: https://doi.org/10.1117/12.2514349 (Accessed May 4, 2019).

Hamamatsu (2017): G8931 Series. Available online at: http://www.hamamatsu.com/resources/pdf/ssd/g8931_series_kapd1018e.pdf (Accessed February 22, 2018).

Headwall (2018): Available online at: http://www.headwallphotonics.com/spectral-imaging/hyperspectral/nano-hyperspec (Accessed Feb. 10, 2018).

Hemmati, H. (2009): *Near-Earth Laser Communications*, Boca Raton, FL: CRC Press.

Hemmati, H. and Caplan, D. (2013): Optical Satellite Communications. *Optical Fiber Telecommunications, Vol. VIB: Systems and Networks*. Oxford, UK: Elsevier, pp. 121–162.

Hubanks, P. A. et al. (2008): MODIS Atmosphere L3 Gridded Product Algorithm Theoretical Basis Document, *ATBD Ref. No.: ATBD-MOD-30*, Vol. 30, p. 96.

Jono, T. et al. (2006): OICETS On-Orbit Laser Communication Experiments, in *Free-Space Laser Communication Technologies XVIII*. Available online at: https://doi.org/10.1117/12.673751 (Accessed May 4, 2019).

Kaslow, D. et al. (2014): Integrated Model-Based Systems Engineering (MBSE) Applied to the Simulation of a CubeSat Mission, in *Proc. Aerospace Conf., 2014 IEEE*, Big Sky, MT, Mar. 1–8. Available online at: https://ieeexplore.ieee.org/stamp/stamp.jsp?tp=&arnumber=6836317 (Accessed May 4, 2019).

Kingsbury, R., Caplan, D., and Cahoy, K. (2015): Compact Optical Transmitters for CubeSat Free-Space Optical Communications, in *Free-Space Laser Communication and Atmospheric Propagation XXVII*. Available online at: https://doi.org/10.1117/12.2080122 (Accessed May 4, 2019).

Kingsbury, R. W. (2015): Optical Communications for Small Satellites, PhD thesis, Massachusetts Institute of Technology, Cambridge, MA.

Kolev, D. R. and Toyoshima, M. (2017): Received-Power Fluctuation Analysis for LEO Satellite-To-Ground Laser Links. *J. Lightwave Tech.*, Vol. 35 (1), pp. 103–112.

Kovalik, J., Farr, W., and Piazzolla, S. (2015): Laser Communications Subsystem for Interplanetary

CubeSats, poster at Interplanetary Small Satellite Conference (ISSC), Santa Clara, CA, Apr. 27–28.

Lesh, J. and Robinson, D. (1986): A Cost-Performance Model for Ground-Based Optical Communications Receiving Telescopes. *Telecommunications and Data Acquisition Rept.*, Vol. N87-15329 07-32, pp. 56–64.

Mandl, D. et al. (2015): Hyperspectral Cubesat Constellation for Rapid Natural Hazard Response, in *Proc. Am. Geophysical Union (AGU) 2015 Fall Meeting*, San Francisco, CA, Dec. 14. Available online at: https://ntrs.nasa.gov/archive/nasa/casi.ntrs.nasa.gov/20150023589.pdf (Accessed May 4, 2019).

Masterson, R. A. and Miller, D. W. (2004): Dynamic Tailoring and Tuning for Precision Optical Space Structures, in *45th AIAA/ASME/ASCE/AHS/ASC Structures, Structural Dynamics and Materials Conf.*, Palm Springs, CA, Apr. 19–22.

Mathason, B. et al. (2019): CubeSat Lasercom Optical Terminals for Near-Earth to Deep Space Communications, in *Proc. SPIE LASE*, Free-Space Laser Communication and Atmospheric Propagation XXXI, Int. Soc. for Optics and Photonics, Vol. 10910, Mar. 6, p. 1091005.

Mathworks (2018): Global Optimization Toolbox Users Guide. Available online at: https://www.mathworks.com/help/pdf_doc/gads/gads_tb.pdf (Accessed Mar. 2018).

Meade (2018): Available online at: https://www.meade.com/telescopes/optical-tube-assembly-ota.html (Accessed Feb. 9, 2018).

NASA (2018): NASA Earth Observatory Cloudy Earth Image of the Day. Available online at: https://earthobservatory.nasa.gov/IOTD/view.php?id=85843 (Accessed May 3, 2018).

Nugent, P. W., Shaw, J. A., and Piazzolla, S. (2013): Infrared Cloud Imager Development for Atmospheric Optical Communication Characterization, and Measurements at the JPL Table Mountain Facility. *Inter-Planetary Network Prog. Rept.*, Vol. 42 (192), pp. 1–31.

Optics, P. R. (2018): OFS935C Fusion Splicer. Available online at: http://www.fiberoptic.com/mmfiberoptic/PDFs/OFS-935C.pdf (Accessed May 18, 2018).

PlaneWave (2018): Available online at: http://planewave.com/products-page/ (Accessed Feb. 20, 2018).

Princeton (2017): PAR Series High Sensitivity APD Front-End Receiver Modules. Available online at: https://www.princetonlightwave.com/wp-content/uploads/2017/01/PAR.pdf (Accessed Mar. 1, 2018).

Riesing, K., Yoon, H., and Cahoy, K. (2017): A Portable Optical Ground Station for Low-Earth Orbit Satellite Communications, in Proc. Int. Conf. on Space Optical Systems and Applications, Nov. 14–16, Naha, Japan. Available online at: https://ieeexplore.ieee.org/stamp/stamp.jsp?tp=&arnumber=8357219 (Accessed May 4, 2019).

Robinson, B. et al. (2018): TeraByte InfraRed Delivery (TBIRD): A Demonstration of Large-Volume Direct-To-Earth Data Transfer from Low-Earth Orbit, in *Free-Space Laser Communication and Atmospheric Propagation XXX*. Available online at: https://www.spiedigitallibrary.org/proceedings/Download?fullDOI=10.1117%2F12.2295023 (Accessed May 4, 2019).

Rowen, D. and Dolphus, R. (2013): 3-Axis Attitude Determination and Control of the AeroCube—4 CubeSats, in *Proc. 27th AIAA/USU Conf. on Small Satellites*, Logan, UT.

Rowen, D. et al. (2016): OCSD-A / AeroCube-7: A Status Update, in 13th *Cal Poly CubeSat Developer's Workshop*, San Luis Obispo, CA, Apr. 20–22. Available online at: https://doi.org/10.1117/12.2295023 (Accessed May 4, 2019).

Sankararaman, S. (2016): Uncertainty Reduction Using Bayesian Inference and Sensitivity Analysis: A Sequential Approach to the NASA Langley Uncertainty Quantification Challenge, in *Proc. 18th AIAA Non-Deterministic Approaches Conf.*, SCITECH Conference, San Diego, CA, Jan. 4–8, p. 1194. Available online at: https://ntrs.nasa.gov/archive/nasa/casi.ntrs.nasa.gov/20150023452.pdf (Accessed May 4, 2019).

Serra, P., Barnwell, N., and Conklin, J. W. (2015): A Novel, Low Power Optical Communication Instrument for Small Satellites, in *Proc. 29th AIAA USU Conf. on Small Satellites*, Logan, UT. Available online at: https://digitalcommons.usu.

edu/cgi/viewcontent.cgi?article=3328&context=smallsat (Accessed May 4, 2019).

Shaw, G. B., Miller, D. W., and Hastings, D. E. (1999): The Generalized Information Network Analysis Methodology for Distributed Satellite Systems, PhD thesis, Citeseer, Massachusetts Institute of Technology, Cambridge, MA.

Shaw, G. B., Miller, D. W., and Hastings, D. E. (2001): Development of the Quantitative Generalized Information Network Analysis Methodology for Satellite Systems. *J. Spacecraft and Rockets*, Vol. 38 (2), pp. 257–269.

Sinclair, D. and Riesing, K. (2017): The Rainbow Connection—Why Now Is the Time for SmallSat Optical Downlinks, in *Proc. 31st AIAA/USU Conf. on Small Satellites*, Logan, UT. Available online at: https://digitalcommons.usu.edu/cgi/viewcontent.cgi?article=3605&context=smallsat (Accessed May 4, 2019).

Sondecker IV, G. R. (2011): Identification and Evolution of Quantities of Interest for a Stochastic Process View of Complex Space System Development, PhD thesis, Massachusetts Institute of Technology, Cambridge, MA.

Spangelo, S. and Cutler, J. (2012): Optimization of Single-Satellite Operational Schedules Towards Enhanced Communication Capacity, in *Proc. AIAA Guidance, Navigation, and Control Conf.*, Minneapolis, MN, Aug. 13–16.

Spangelo, S. C. et al. (2013): Model Based Systems Engineering (MBSE) Applied to Radio Aurora Explorer (RAX) CubeSat Mission Operational Scenarios, in *Proc. Aerospace Conf., 2013 IEEE*. Available online at: https://doi.org/10.1109/AERO.2013.6496894 (Accessed May 4, 2019).

Spangelo, S. C. et al. (2012): Applying Model Based Systems Engineering (MBSE) to a Standard CubeSat, in *Proc. Aerospace Conf., 2012 IEEE*. Available online at: https://doi.org/10.1109/AERO.2012.6187339 (Accessed May 4, 2019).

Stout, K. D. (2015): Bayesian-Based Simulation Model Validation for Spacecraft Thermal Systems, PhD thesis, Massachusetts Institute of Technology, Cambridge, MA.

Takenaka, H. et al. (2016): In-Orbit Verification of Small Optical Transponder (SOTA): Evaluation of Satellite-To-Ground Laser Communication Links, in *Free-Space Laser Communication and Atmospheric Propagation XXVIII*. Available online at: https://doi.org/10.1117/12.2214461 (Accessed May 4, 2019).

Thorlabs (2010): *4.7 Mm Focal Length Fiber Pigtail Collimator*, Thorlabs Inc. (Rev. C ed.), drawing 17382-E01, Part number CFS5-1550-APC.

Voxtel (2015): Voxtel Catalog: Photodiodes, APDs, Photoreceivers, LRF Receivers. Available at: http://voxtel-inc.com/files/Voxtel-Catalog.pdf (Accessed May 18, 2018).

White, C. et al. (2012): System Verification of MSL Skycrane Using An Integrated ADAMS Simulation, in *Proc. Aerospace Conf., 2012 IEEE*, Big Sky, MT, Mar. 3–10, pp. 1–11. Available online at: https://trs.jpl.nasa.gov/bitstream/handle/2014/45011/12-0208_A1b.pdf?sequence=1&isAllowed=y (Accessed May 4, 2019).

Wilson, K. et al. (2012): Development of the Optical Communications Telescope Laboratory: A Laser Communications Relay Demonstration Ground Station, in *Proc. International Conference on Space Optical Systems (ICSOS)*, Ajaccio, Corsica, FR, Oct. 9–12. Available online at: https://trs.jpl.nasa.gov/bitstream/handle/2014/43098/12-3507_A1b.pdf?sequence=1&isAllowed=y (Accessed May 4, 2019).

Win, M. Z. (1989): Estimation and Tracking for Deep-Space Optical Communications, in *Proc. OE/LASE'89*, Int. Soc. for Optics and Photonics, Los Angeles. CA (15–20 Jan.), pp. 80–87. Available online at: https://doi.org/10.1117/12.951698 (Accessed May 4, 2019).

Win, M. Z. and Chen, C. C. (1992): Analysis of a Spatial-Tracking Subsystem for Optical Communications, in *Proc. OE/LASE'92*, Free-Space Laser Communication Technologies IV, Int. Soc. for Optics and Photonics, Vol. 1635, Jun. 9, pp. 318–325. doi: 10.1117/12.59287.

Winick, K.A. (1986): Atmospheric Turbulence-Induced Signal Fades on Optical Heterodyne Communication Links. *Applied Optics*, Vol. 25 (11), pp. 1817–1825.

Wysocki, P., Wood, T., Grant, A. et al. (2006): High Reliability 49 DB Gain, 13 W PM Fiber Amplifier

at 1550 Nm with 30 DB PER and Record Efficiency, in *Proc. Optical Fiber Communication Conf.*, Optical Society of America, p. PDP17.

Yao, W. et al. (2011): Review of Uncertainty-Based Multidisciplinary Design Optimization Methods for Aerospace Vehicles. *Progress in Aerospace Sciences*, p. PDP17, Vol. 47 (6), pp. 450–479.

Zarifian, P. et al. (2015): Team Xc: JPL's Collaborative Design Team for Exploring CubeSat, NanoSat, and SmallSat-Based Mission Concepts, in *Proc. Aerospace Conf., 2015 IEEE*, Big Sky, MT, Mar. 1–8, 2014. Available online at: https://doi.org/10.1109/AERO.2015.7119221 (May 4, 2019).